MRS Advances (2022) 7:886–891
https://doi.org/10.1557/s43580-022-00327-x

ORIGINAL PAPER

Passive film analysis and corrosion study of steel type 301 after mechanical deformation

Temitope Olumide Olugbade[1]

Received: 16 June 2022 / Accepted: 19 July 2022 / Published online: 4 August 2022

Abstract

The electrochemical properties of the passive film formed on surface-modified 301 stainless steel (SS) were examined in the present study. After surface treatment, the passive film analysis was carried out via X-ray photoelectron spectroscopy (XPS) technique, while the surface microstructure of the samples was examined by scanning electron microscope analysis. With Cr 2p, Fe 2p, O 1s, Ni 2p, and C 1s as the principal spectra in the passive film, the Cr 2p spectrum shows two major peaks at 574.3 eV and 583.8 eV corresponding to Cr $2p_{3/2}$ (Cr in the metallic state) and Cr $2p_{1/2}$, respectively. The Fe 2p spectrum has two major peaks of 707.1 and 720.1 eV corresponding to Fe $2p_{3/2}$ (Fe in metallic state) and Fe $2p_{1/2}$ peaks, respectively, while the binding energies of 853.3 and 875.1 eV for the Ni 2p spectrum correspond to nickel in the metallic state. The XPS spectra revealed a higher percentage of Cr in the passive film of the treated 301 SS when compared with other elements. From the polarization results, the treated 301 SS possessed a lower corrosion current density of 1.401 mA/cm^2 and higher corrosion potential of − 0.085 V.

Introduction

After surface modification, the study on the passive film analysis and general corrosion property of stainless steels is presently receiving wide attention for many engineering applications. To a large extent, characterizing the passive layers formed on steel type 301 steel goes a long way in determining its corrosion resistance performance which will compliments its inherent properties (high hardness and strength). Moreover, these properties can be enhanced via surface treatments or modifications [1–3] under the right atmospheric conditions and with appropriate processing parameters.

Several methods of surface modifications such as ultrasonic peening, surface mechanical attrition treatment (SMAT), and many more [1, 4–6], have been adopted in the past to enhance the surface properties of metallic materials. Compared to other forms of surface modification such as machining, heat treatments, coatings, or electrodepositions [7–12], SMAT has been recognized as an important tool for generating nanocrystalline layers on the material surface and refining the microstructure to nanoscale level, thereby significantly improving the overall properties without affecting the original composition of the material. Over the years, the SMAT system has been successfully applied to different materials systems including Al, Ti, Co, Fe, Cu, Mg, stainless steels, and many more [13–18]. The positive feedbacks on stainless steels from previous studies coupled with the fact that the material's inherent properties are not often tampered with necessitated the choice of SMAT as the surface modification method in the present study.

The methods of surface nanocrystallization adopted could influence the corrosion resistance of materials to a large extent [19–26]. For instance, surface treatment by equal channel angular processing (ECAP) has been shown to enhance the corrosion resistance of nanocrystalline 304 steel [27], while the corrosion resistance of 409 steel decreased after surface treatment by SMAT at various processing times following the increase in microstrain during treatment [15]. This indicates that the corrosion properties largely depend on the nature and type of surface treatments, processing parameters, environmental conditions, etc. [28–31].

The present study characterizes the passive film formed on steel type 301 after mechanical deformation via SMAT and determine its aftermath corrosion properties. The surface microstructure of the untreated and treated samples was

✉ Temitope Olumide Olugbade
tkolugbade@futa.edu.ng

[1] Department of Industrial and Production Engineering, Federal University of Technology, P.M.B. 704, Akure, Ondo State, Nigeria

characterized by scanning electron microscope (SEM). The corrosion resistance behaviour was studied by polarization tests and electrochemical impedance spectroscopy (EIS) analysis. The elemental composition of the passive film formed after surface mechanical treatment was characterized by the X-ray photoelectron spectroscopy (XPS) technique.

Experimental

Materials

A commercial steel type 301 was used in the present study with a chemical composition of (wt%) Cr: 18.00; Ni: 10.00; C: 0.15; Mn: 2.00; Si: 1.00; S: 0.03; P: 0.05; Fe: bal. The sample subjected to SMAT on both surfaces was treated for 300 s. The SMAT process has been explained in detail in previous studies [4, 19, 32–34]. The morphology of both samples were observed by a Scanning Electron Microscope (FEI Quanta 450 FEG SEM). The composition of the passive layer obtained after treatment was studied using X-ray photoelectron spectroscopy (XPS PHI5082, Japan), with an initial photon energy of 1486.6 eV.

Corrosion tests

The corrosion behaviour of the untreated and treated samples was investigated by electrochemical tests carried out in 0.6 M NaCl solution using Thales Z3.04 USB electrochemical workstation (Germany). Th corrosion tests were carried out adopting the conventional three-electrode cell

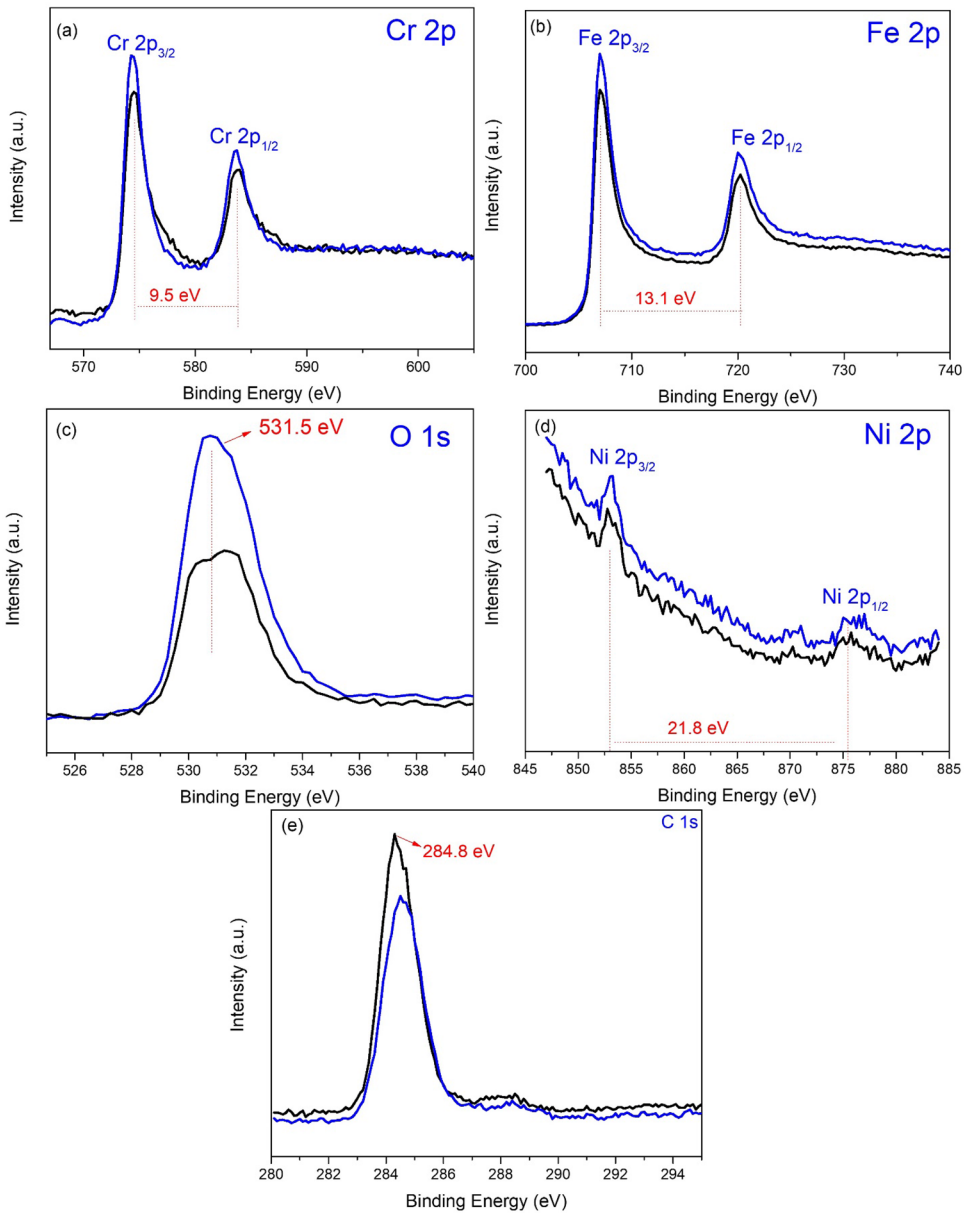

Fig. 1 XPS spectra of the passive films formed on the treated 301 SS: **a** Cr 2p, **b** Fe 2p, **c** O 1s, **d** Ni 2p, **e** C 1s

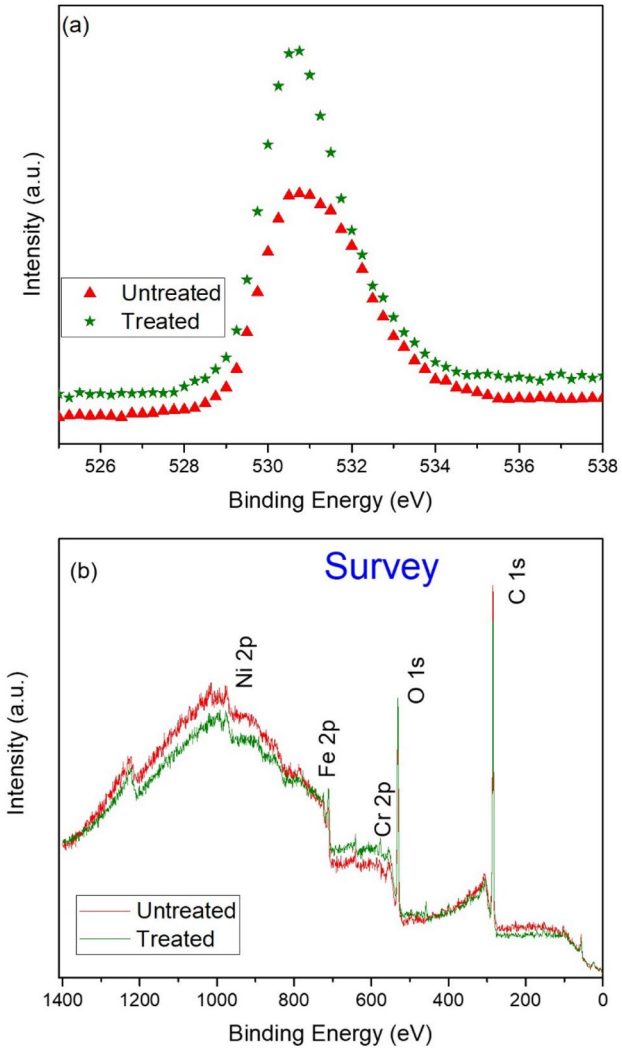

Fig. 2 XPS analysis of both untreated and treated 301 SS samples: **a** Cr 2p core-level spectra and **b** XPS survey spectra

system with silver/silver chloride as the reference electrode, platinum as the counter electrode, and the samples as the working electrode. After the open circuit potential (OCP), potentiodynamic polarization test was carried out to measure the corrosion potential (E_{corr}) and corrosion current density (i_{corr}) of the untreated and treated samples. The test was completed at a scan rate of 1 mV/s, in the potential range from − 0.1 to + 0.12 V. The electrochemical impedance spectroscopy (EIS) study was utilized to compare the impedance behaviour difference between the untreated and treated samples, over the frequencies range from 100 mHz to 100 kHz with an amplitude of 10 mV. The electrochemical studies were repeated three times and the EIS parameters with equivalent circuit models were determined from the Nyquist plot after fitting the data using EIS spectrum analyzer software.

Results and discussions

The XPS spectra of Cr 2p, Fe 2p, O 1s, Ni 2p, and C 1s of the passive films formed on the treated 301 steel are shown in Fig. 1a–e, respectively. In Fig. 1, similar peaks located at the same binding energy were observed for both untreated (designated by the black curves) and treated 301 steel (designated by the blue curves); however, a higher intensity was obtained for the treated sample. For the high-resolution XPS spectrum of Cr (Fig. 1a), two peaks are seen at 574.3 eV and 583.8 eV corresponding to Cr $2p_{3/2}$ and Cr $2p_{1/2}$, respectively [35–37] with the difference of 9.5 eV between the peaks. However, the Cr $2p_{3/2}$ peak can be related to chromium (Cr) in the metallic state. The Fe 2p spectrum (Fig. 1b) shows two main peaks at 707.1 and 720.1 eV which can be ascribed to Fe $2p_{3/2}$ and Fe $2p_{1/2}$, respectively [38, 39], with 13.1 eV apart the peaks. The Fe $2p_{3/2}$ peak can likewise be ascribed to iron (Fe) in the metallic state. The O 1s spectrum (Fig. 1c) is centred at 531.5 eV [40] which is related to oxygen vacancies, while the Ni 2p spectrum (Fig. 1d) shows two major peaks at 853.3 and 875.1 eV which can be attributed to nickel (Ni) metal [41, 42], with 21.8 eV separating the peaks.

Moreover, an additional small peak at binding energy of 872 eV in Fig. 1d is a shakeup satellite of Ni$2p_{1/2}$ peak. Meanwhile, the C 1s spectrum (Fig. 1e) is centred at 284.8 eV. As indicated in Fig. 2, the Cr 2p core-level spectra revealed a higher signal (Fig. 2a) and the XPS survey spectra (Fig. 2b) for the treated sample compared with the untreated sample.

The treated sample exhibited an increase in Cr content when compared to the untreated sample. Five main peaks located at 853.3, 707.1, 531.5, 574.3, and 284.8 eV relating to Ni 2p, Fe 2p, O 1s, Cr 2p, and C 1s, respectively, can be seen (Fig. 2b). Figure 3a–d shows the potentiodynamic polarization curves, Nyquist plot, impedance plot and phase angle plots for the untreated and treated 301 steel sample in 0.6 M NaCl solution. The corrosion current density (i_{corr}) and potential (E_{corr}) values were obtained from the polarization curves through the Tafel extrapolation method. As indicated in Fig. 3a, compared to the untreated sample with the corrosion current density value of 2.778 mA/cm^2, the treated sample exhibited a reduced corrosion density value of 1.401 mA/cm^2. Likewise, the untreated sample possessed

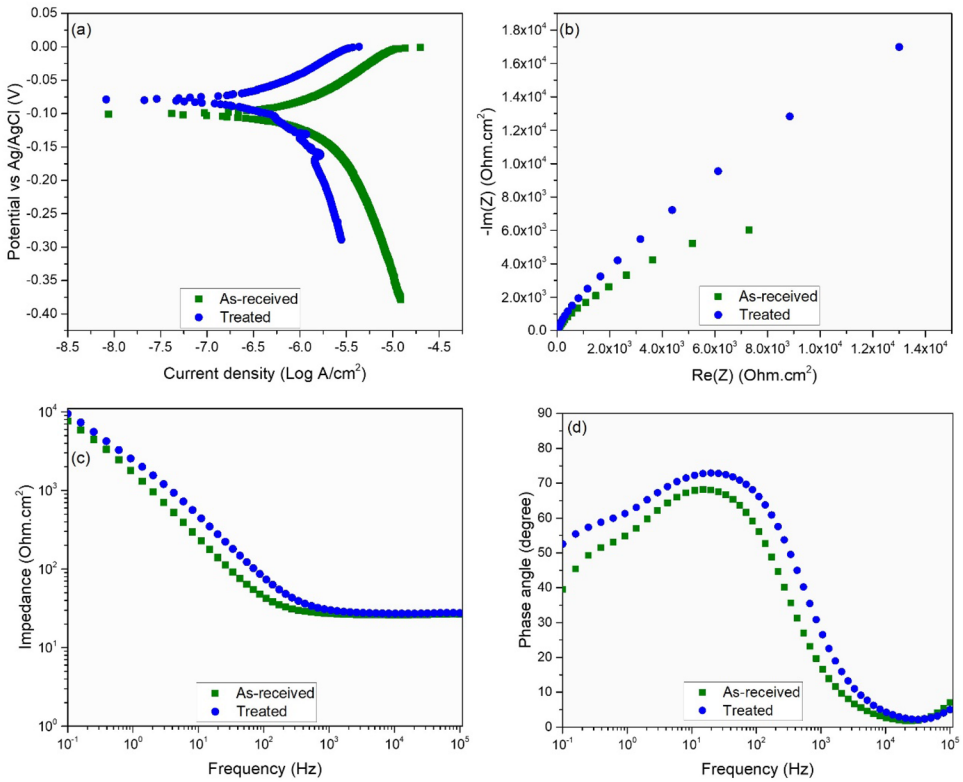

Fig. 3 Potentiodynamic polarization curves and EIS plots for the untreated and treated 301 SS samples in NaCl solution: **a** polarization curve, **b** the Nyquist, **c** Bode impedance, and **d** Bode phase angle plots

an E_{corr} value of − 0.095 V, whereas a higher corrosion potential of − 0.085 V was obtained for the treated sample, hence an improvement in corrosion resistance. These observations show the positive influence of surface treatment by SMAT on the corrosion behaviour of 301 SS.

As revealed in the EIS analysis, the larger diameter of capacitive semicircle for the treated sample (Fig. 3b) indicates the formation of more dense passive films on the sample surface, hence an improved corrosion resistance for the treated samples. The improved corrosion resistance is also substantiated by the increase in the impedance (Fig. 3c) and phase angle (Fig. 3d) for the treated sample. After surface treatment, the corrosion resistance of the untreated and treated samples was compared in 0.6 M NaCl aqueous solution. The SEM micrograph revealed a better corrosion resistance for the treated sample (Fig. 4b) as compared to the untreated sample (Fig. 4a).

The passive film is characterized with Cr 2p, Fe 2p, O 1s, Ni 2p, C 1s as the principal elements. In general, the impact of surface mechanical treatment largely depends on the processing time, nature and type of materials, the materials of the ball used, the quantity and size of the balls, as well as the power voltage [21–27].

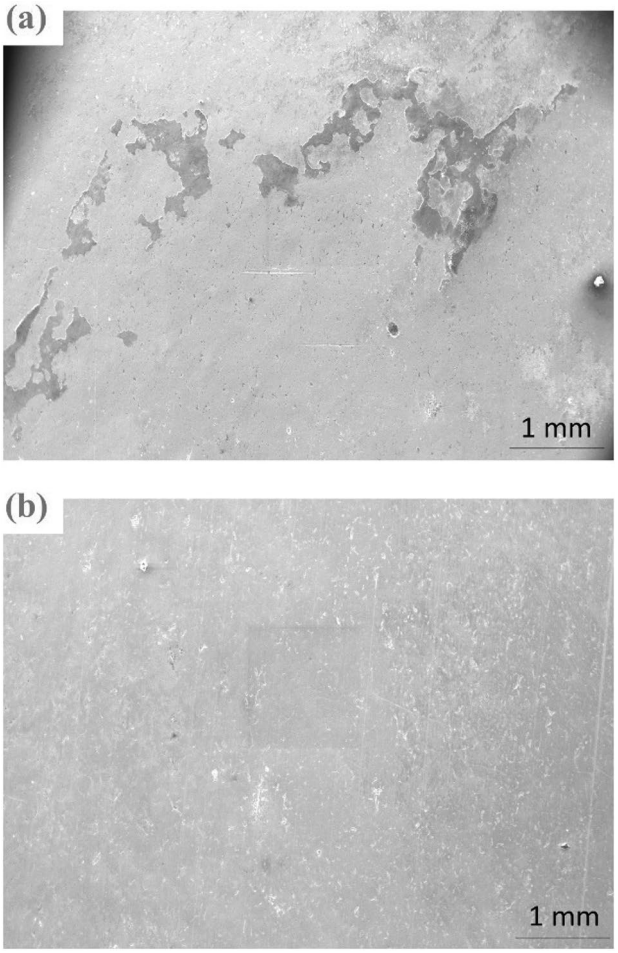

Fig. 4 SEM images of untreated and treated 301 SS samples, after polarization in sodium chloride solution: **a** untreated and **b** treated

Conclusion

The passive films formed on the surface of 301 SS after surface treatment were characterized via X-ray photoelectron spectroscopy (XPS) technique, polarization studies, EIS analysis, and scanning electron microscopy (SEM) analysis. The elemental composition of the passive film characterized by XPS technique revealed the presence of Cr, Fe, O, Ni, C as the main elements in the passive film for both samples, with a higher level of Cr content in the treated sample as compared with that of the untreated one. The Cr 2p spectrum shows two major peaks at 574.3 eV and 583.8 eV corresponding to Cr $2p_{3/2}$ and Cr $2p_{1/2}$, respectively. For the high-resolution XPS spectrum of Fe, two peaks are seen at 707.1 and 720.1 eV which can be ascribed to Fe $2p_{3/2}$ and Fe $2p_{1/2}$, respectively, while the Ni 2p spectrum shows two main peaks at 853.3 and 875.1 eV which can be linked to Ni $2p_{3/2}$ and Ni $2p_{1/2}$, respectively. The C 1s and O 1s spectra are centred at 284.8 and 531.5 eV, respectively. The electrochemical tests revealed that the treated 301 SS possessed a corrosion potential of − 0.085 V and a corrosion current density of 1.401 mA/cm^2.

Acknowledgments The author appreciates the support of the Centre for Advanced Structural Materials (CASM), Hong Kong SAR, as regards the SMAT technique.

Data availability The data that support the findings of this study are available on request from the author.

Declarations

Conflict of interest The author reports no conflict of interest.

References

1. Y. Lu, X. Liu, L. Wang, J. Yang, H. Xu, J. Ocean. Limnol. (2022). https://doi.org/10.1007/s00343-021-1168-9
2. Y. Lin, J. Lu, L. Wang, T. Xu, Q. Xue, Acta Mater. **54**, 5599 (2006)
3. M.A.M. Ibrahim, S.S. Abd El Rehim, M.M. Hamza, Mater. Chem. Phys. **115**, 80–85 (2009)
4. N.R. Tao, M.L. Sui, J. Lu, K. Lu, Nanostruct. Mater **11**, 433 (1999)
5. X. Wu, N. Tao, Y. Hong, B. Xu, J. Lu, K. Lu, Acta Mater. **50**, 2075 (2002)
6. Z.C. Wang, F. Di-Franco, A. Seyeux, S. Zanna, V. Maurice, P. Marcus, J. Electrochem. Soc. **166**, C3376–C3388 (2019)
7. C. Dang, T.O. Olugbade, S. Fan, H. Zhang, L.L. Gao, J. Li, Y. Lu, Vacuum **156**, 310–316 (2018)
8. C. Dang, Y. Yao, T.O. Olugbade, L. Li, L. Wang, Thin Solid Films **653**, 107–112 (2018)
9. H. Zu, K. Chau, T.O. Olugbade, L. Pan, D.H. Chow, L. Huang, L. Zheng, W. Tong, X. Li, Z. Chen, X. He, R. Zhang, J. Mi, Y. Li, B. Dai, J. Wang, J. Xu, K. Liu, J. Lu, L. Qin, J. Mater. Sci. Technol. **63**, 145–160 (2021)
10. T.E. Abioye, I.S. Omotehinse, I.O. Oladele, T.O. Olugbade, T.I. Ogedengbe, World J. Eng. **17**, 87–96 (2020)
11. T.E. Abioye, T.O. Olugbade, T.I. Ogedengbe, J. Emerg. Trends Eng. Appl. Sci. **8**, 225 (2017)
12. T.O. Olugbade, O.O. Omoniyi, B.O. Omiyale, J. Inst. Eng. (India): Ser. D **103**, 141–147 (2022)
13. K. Wang, N.R. Tao, G. Liu, J. Lu, K. Lu, Acta. Mater. **54**, 5281 (2006)
14. T. Olugbade, Data Brief **25**, 104033 (2019)
15. T. Balusamy, S. Kumar, T.S.N. Sankara Narayanan, Corros. Sci. **52**, 3826–3834 (2010)
16. T. Balusamy, T.S.N. Sankara Narayanan, K. Ravichandran, I.S. Park, M.H. Lee, Corros. Sci. **74**, 332–344 (2013)
17. T.O. Olugbade, Anal. Lett. **54**, 1055–1067 (2021)
18. T.I. Ogedengbe, T.O. Olugbade, O. Olagunju, Br. J. Appl. Sci. Technol. **10**, 1–11 (2015)
19. N.R. Tao, J. Lu, K. Lu, Mater. Sci. Forum **579**, 91–108 (2008)
20. T.O. Olugbade, J. Lu, Anal. Lett. **52**, 2454–2471 (2019)
21. H.Q. Sun, Y.N. Shi, M.X. Zhang, K. Lu, Acta Mater. **55**, 975 (2007)
22. T.O. Olugbade, J. Lu, Nano Mater. Sci. **2**, 3–31 (2020)
23. T.O. Olugbade, O.T. Ojo, B.O. Omiyale, E.O. Olutomilola, B.J. Olorunfemi, J. Braz. Soc. Mech. Sci. Eng. **43**, 421 (2021)

24. T. Mohammed, T.O. Olugbade, I. Nwankwo, J. Sci. Res. Rep. **10**, 1–9 (2016)
25. T. Olugbade, J. Lu, in *Twelfth International Conference on Fatigue Damage of Structural Materials, Cape Cod, Hyannis* (2018)
26. T.O. Olugbade, Corros. Rev. **38**, 473–488 (2020)
27. Z.J. Zheng, Y. Gao, Y. Gui, M. Zhu, Corros. Sci. **54**, 60–67 (2012)
28. T.O. Olugbade, T.E. Abioye, P.K. Farayibi, N.G. Olaiya, B.O. Omiyale, T.I. Ogedengbe, Anal. Lett. **54**, 1588–1602 (2021)
29. H.W. Chang, P.M. Kelly, Y.N. Shi, M.X. Zhang, Surf. Coat. Technol. **206**, 3970–3980 (2012)
30. T.O. Olugbade, B.O. Omiyale, O.T. Ojo, J. Mater. Eng. Perform. **31**, 1707–1727 (2022)
31. T.O. Olugbade, E.O. Olutomilola, B.J. Olorunfemi, Corros. Rev. (2022). https://doi.org/10.1515/corrrev-2021-0072
32. T. Olugbade, J. Lu, in *International Conference on Nanostructured Materials* (NANO 2020) Australia, vol. **117** (2020)
33. T.O. Olugbade, Chem. Afr. **5**, 333–340 (2022)
34. T. Olugbade, C. Liu, J. Lu, Adv. Eng. Mater. **21**, 1900125 (2019)
35. I.S. Zhidkov, A.I. Kukharenko, A.V. Makarov, R.A. Savrai, N.V. Gavrilov, S.O. Cholakh, E.Z. Kurmaevs, Surf. Coat. Technol. **386**, 125492 (2020)
36. N. Chung, Spectroscopy **33**, 28–34 (2018)
37. L. Ma, F. Wiame, V. Maurice, P. Marcus, Corros. Sci. **140**, 205–216 (2018)
38. B. Adrien, D. Thomas, D. Nadège, N. Eric, D. Julien, L. Lydia, B. Christine, Surf. Interfaces **22**, 100874 (2021)
39. S. Detriche, S. Vivegnis, J.F. Vanhumbeeck, A. Felten, P. Louette, F. Renner, J. Delhalle, Z. Mekhalif, J. Electron Spectrosc. Relat. Phenom. **243**, 146970 (2020)
40. R. Natarajan, N. Palaniswamy, M. Natesan, V.S. Muralidharan, Open Corros. J. **2**, 114–124 (2009)
41. Z. Duan, F. Arjmand, L. Zhang, H. Abe, J. Nucl. Sci. Technol. **53**, 1435–1446 (2016)
42. M.S. Qurashi, Y. Cui, J. Wang, N. Dong, J. Bai, Y. Wu, P. Han, Int. J. Electrochem. Sci. **14**, 10642–10656 (2019)